Photoemission studies of crystalline and amorphous Sb_2Se_3

Z. Hurych, D. Davis, D. Buczek, and C. Wood*
Physics Department, Northern Illinois University, DeKalb, Illinois 60115

G. J. Lapeyre† and A. D. Baer
Physics Department, Montana State University, Bozeman, Montana 59715
(Received 16 November 1972; revised manuscript received 26 November 1973)

The photoemission energy distribution curves (EDC's) of crystalline and amorphous Sb_2Se_3 were measured in the photon energy range $h\nu = 7$ to 35 eV using polarized radiation from a synchrotron storage ring. The polarization dependence of the EDC's is much stronger than that of the reflectance spectra. The EDC's show several regions of high density of states in both the valence and conduction bands, with the structure strongly smeared-out in amorphous Sb_2Se_3. The region of the upper 2 eV of the valence band with six electrons per Sb_2Se_3 molecule attributed primarily to the selenium lone p pairs, is clearly separated from the remaining part of the EDC's in crystalline Sb_2Se_3. The optical transitions in crystalline Sb_2Se_3 occur with matrix elements strongly dependent on the orientation of the electrical vector of the polarized radiation as a result of crystal-field effects. Model densities of states are constructed for both crystalline and amorphous Sb_2Se_3.

I. INTRODUCTION

Sb_2Se_3 belongs to V-VI compound semiconductors, a group of materials whose optical and transport properties have been widely investigated. However, there is available little data on band structure of these compounds owing to the complicated primitive cell (comprised of 112 valence electrons in the case of Sb_2Se_3), and the density-of-states models are generally derived from the molecular-orbital approach, with the bonding and weakly bonding bands usually adjusted to fit the reflectance spectra.[1]

The typical features of the reflectance spectra of these compounds in both crystalline and amorphous forms are two reflectivity bands, the first occurring in the near-ir and visible region, and the second in the vacuum-uv region of the spectrum,[2-4] with onset at ~7 eV in the case of Sb_2Se_3. These two reflectivity bands are usually interpreted[1,4] as originating from splitting of the valence band into strongly bonding and weakly bonding states. Kastner[5] has recently pointed out the important role of the lone (unshared) p electrons of chalcogen atoms in forming the weakly bonding band in these compounds. More detailed knowledge of the valence-band structure, particularly its upper part formed by the lone-pairs, should be useful in explaining many physical properties of these materials. However, the above reflectivity-based model is of rather conjectural character, since the reflectivity (and associated optical constants) provide information on the joint density of states (JDOS) only, without determining absolutely either the initial or the final energy of states involved. In addition, it is generally difficult to determine which structure in the optical data is due to the band density of states and which is due to enhancement by the critical points in JDOS or by matrix elements, although the critical-points contribution is generally unimportant in amorphous materials as a result of the lack of long-range order. This question of matrix elements is further complicated by the low symmetry of these crystals, since some transitions could be either allowed or prohibited by the symmetry of the initial and final states. Such effects should show up when polarized light is used where the matrix elements would depend, in general, both on the wave vector $\vec{k}$ and on the orientation of the electrical vector $\vec{E}_0$.

We have employed photoemission spectroscopy, which is capable of locating the absolute position of structures in either valence or conduction band, to substantially refine the existing density-of-states model and to obtain information on the character of the matrix elements. Owing to the high resolution (0.2 eV), we have been able to determine several fundamental features in the upper (i.e., weakly bonding) valence band as well as a conduction-band structure, unresolved previously in the x-ray photoemission studies.[6] Application of polarized radiation from the synchrotron storage ring also reveals a strong effect of the crystal field which shows up as a strong dependence of the energy distribution curves (EDC's) on the orientation of $\vec{E}_0$.

II. EXPERIMENTAL

A. Photoemission apparatus and light source

The 240-MeV storage ring of synchrotron radiation at the Physical Science Laboratory of the University of Wisconsin was used as a continuum light source. The beam was focused at the entrance slit of a monochromator optically equivalent to the McPherson 225 model. Upon reflection and dispersion at the grating, the beam is focused at the exit slit of the monochromator and

then diverges again ($f = 10.4$). Therefore, an elliptical mirror was used to refocus the light beam to a spot of approximately 1 mm in diameter which illuminated the sample. Even though the beam is naturally polarized in the median plane of the storage ring, some depolarization occurs after reflections at focusing mirrors and the grating. The polarization of the light illuminating the sample was estimated to be ~80%. [This estimate is based on polarization measurements on an optically equivalent monochromator; C. G. Olson (private communication).]

A double-pass, cylindrical, electrostatic mirror with a spiraltron electron multiplier was used as an electron-energy analyzer. This analyzer, which is described in detail elsewhere,[7] detects only electrons of a certain velocity and which originate from a small volume (of linear dimensions ~1 mm) surrounding a focal point; the focal point was positioned at the center of the light spot. By moving the sample with respect to the focal point of the analyzer it was possible to select the best surface area of the sample, the criterion being that the ratio of the high-energy end of EDC's to the low-energy peak due to scattering be maximized. For good crystal cleavages and uniform films this was only of secondary importance. The sampling of the velocity of electrons was done by sweeping a retarding or accelerating voltage between two concentric hemispheres located in the region between the electron source and the analyzer entrance. Analyzer resolution was then independent of the electron energy. In the present work the analyzer was set to pass 20-eV electrons and the resolution was 0.2 eV for all electron energies. This pass energy gave the most favorable condition for high transmittance of the analyzer while retaining good resolution. (Since this mode of analyzer operation has been used by several UPS groups, it is appropriate to note here that the use of the constant resolution mode results, however, in an energy-dependent transmission of the analyzer when the object point has a finite size. This results from the fact that electrons originating off center of the concentric hemispheres have both normal as well as tangential components of velocity producing electron refraction.) Digital processing of the signal at the output of the channeltron eliminated the vibrational, electrical, and Johnson noise; the dark count was less than 1 count per sec. The primary source of noise was the statistical error, which was 1% of full scale or better. This resulted in the necessity of a longer counting time for $h\nu > 20$ eV, where the light intensity began to decrease.

B. Sample preparation

Orthorhombic single crystals of Sb_2Se_3 (space group D_{2h}^{16}, $a = 11.62$ Å, $b = 11.77$ Å, $c = 3.96$ Å) were grown from the melt in a horizontal zone refiner by the method described in Ref. 8 from 99.9999%-purity elements. Samples ~$9 \times 9 \times 3$ mm were cut from ingots ~$\frac{1}{2}$-in. in diameter and 10-in. long. The base pressure in the photoemission chamber was 8×10^{-10} torr and did not change substantially during the cleaving. Excellent mirror-like cleaved surfaces perpendicular to $\hat{b}$ were obtained which enabled the sample to be illuminated with $\vec{E}_0 \| \hat{a}$ or $\vec{E}_0 \| \hat{c}$, respectively. ($\vec{E}_0$ is the electric vector of polarized light.) The sample was positioned in such a manner that the incident light was always s polarized; i.e., $\vec{E}_0$ was parallel only with one of the three orthorhombic axes at a time.

Amorphous Sb_2Se_3 films of thickness ~200–500 Å were prepared *in situ* by evaporation of Sb_2Se_3 from an electron-beam gun at very low rates (~1 Å/sec) onto nickel and quartz substrates with Pt contacts. This method of evaporation had been developed earlier[9] to produce amorphous stoichiometric Sb_2Se_3 films within ~1% error in composition as determined by electron microprobe. After the photoemission measurements, the films were checked by x-ray diffraction and were found to be amorphous. The pressure before the evaporation was 5×10^{-10} torr, rising to 4×10^{-9} torr during the evaporation, and decreasing back to 8×10^{-10} torr immediately after the electron-beam gun was turned off.

III. THEORY

Since there are several detailed treatments of the three-step model of the photoemission process,[10–12] only conclusions pertinent to our results will be mentioned here. In addition, some features of photoemission when polarized radiation is used will be discussed qualitatively.

The transition rate for the optical excitation is proportional to the square of the electric dipole matrix elements $M_{if}(h\nu, \vec{k}E_0) = \langle \psi_i | H' | \psi_f \rangle$, where H' is the light perturbation Hamiltonian, $\vec{k}$ is the crystal momentum, and $\vec{E}_0$ is the electrical vector of polarized light. The form of the $\vec{k}$ dependence of M_{if} depends on the character of the wave functions ψ_i and ψ_f in the initial and final states. If these are properly described by Bloch functions, the $\vec{k}$ dependence of M_{if} includes the term $\delta(\vec{k}_i - \vec{k}_f)$ (direct transition), and the excitation is described in terms of M_{if} and the JDOS. If Bloch functions do not properly describe either the initial or final states, the $k_i = k_f$ condition for nonzero M_{if} is relaxed. The optical transitions are then termed nondirect, and their rate can be expressed in terms of M_{if} and band densities of initial and final states.

The dependence of M_{if} on $\vec{E}_0$ arises from the $\vec{A} \cdot \vec{p}$ term in H', $\vec{A}$ being the vector potential of the exciting radiation. The $\vec{E}_0$ dependence can be very

important in an anisotropic solid such as Sb_2Se_3. This $\vec{E}_0$ dependence of M_{if} arises from the symmetry of the initial and final states rather than from the detailed character of ψ_i and ψ_f, reflecting the effect of crystal symmetry and field and can occur both for direct and nondirect transitions. Treatment of this problem in the case of wurtzite CdS can be found in Ref. 13.

In addition to the dependence on $|M_{if}|^2$, the photoemission EDC's depend also on the scattering factor $S(h\nu, k_f, E)$,[10] which describes the transport and escape of electrons excited to final energy E. The $\vec{k}_f$ dependence of S gives rise to an angular dependence of the photoemitted electrons. Several experiments have been performed to investigate this angular dependence of photoemission in the case of Cu,[14] Ag,[15] and Au.[16] In the case of free-electron-like metals this angular dependence of photoemitted electrons has been treated theoretically by Mahan[17] from first principles.

Since $\vec{k}_f$ depends on the oreintation of $\vec{E}_0$ through the $\vec{A}\cdot\vec{p}$ term and some relation between $\vec{k}_i$ and $\vec{k}_f$, it is appropriate to incorporate the $\vec{E}_0$ dependence also into the scattering function $S(h\nu, E, \vec{k}_f, \vec{E}_0)$. The EDC's then include a twofold dependence on the orientation of $\vec{E}_0$ (i) through the probability of optical excitation proportional to $(M_{if})^2$ (at any $h\nu$ the transition can be allowed for one polarization and forbidden for the other as a result of symmetry) and (ii) through the transport and escape function S, where the angular distribution of emitted electrons depends upon $\vec{E}_0$ through the $\vec{k}_f$ dependence on $\vec{E}_0$ as a result of the term $\vec{A}\cdot\vec{p}$. This dependence would generally be much weaker in the case of nondirect transitions for which $k_i \neq k_f$.

While effect (ii) is not generally considered when EDC's are measured using the retarding-field analyzer (which yields an "averaged" angular distribution) it should be considered in the case of directional analyzers, such as the double-pass electrostatic mirror used in this work. It is then desirable to separate the part due to M_{if} and that due to the S dependence on $\vec{E}_0$ in the family of EDC's with different $h\nu$ at constant polarization and constant angle of collection. Since there is no theory similar to that of Mahan,[17] which would treat this problem in the case of complex semiconductors like Sb_2Se_3, we used, as a first approximation, the following criteria for the separation of the M_{if} and S dependence.

(i) The M_{if} dependence on $\vec{E}_0$ can strongly modulate the intensity of peaks in the EDC's as $h\nu$ is varied at constant polarization, since even a small change in $h\nu$ can result in transitions between initial and final states of different symmetry, which could change from allowed to forbidden or vice versa. Peaks in the EDC's may then suddenly appear and disappear when $h\nu$ is changed by a small amount, i.e., the peaks may behave similarly to those in the case of direct transitions.

(ii) Since the angular dependence of S is rather smooth and it is a continuous function of k_f as contrasted to the "0 to 1" type behavior of M_{if} $(\vec{E}_0)$, and since the over-all momentum distribution k_f of all excited electrons would also change with $h\nu$ more gradually than the 0 to 1 changes in M_{if}, one may expect rather weak and gradual modulation of structure in the EDC's due to the $S(k_f, h\nu, E, \vec{E}_0)$ term as $h\nu$ is varied at a given polarization.[18] This $S(k_f, h\nu, E, \vec{E}_0)$ term would be expected to have a very small effect in the case of nondirect transitions.

IV. EXPERIMENTAL RESULTS

The experimental data (EDC's) are presented in Figs. 1–6 for crystalline Sb_2Se_3 for two orientations of the electric vector $\vec{E}_0$ of the polarized light, $\vec{E}_0 \| \hat{c}$, $\vec{E}_0 \| \hat{a}$, and for amorphous Sb_2Se_3. It is seen that the EDC's exhibit a structure which is strongly varying with $h\nu$ in the photon energy range between 7 and 15 eV. At higher photon energies, the structure (peaks, shoulders, valleys) gets progressively less sharp as a result of the increasing contribution of scattered electrons which build a structureless background at the lower-energy part of the EDC's and decrease the signal at the high-energy end. Starting at $h\nu \sim 20$ eV an additional over-all decrease of the signal occurs as a result of decreasing efficiency of the normal-incidence grating monochromator. Therefore, primarily the 7–20 eV region of $h\nu$ was used for further analysis. The EDC's for $h\nu \geq 20$ eV look similar to those for 20 eV but the signal was considerably weaker. The main purpose of taking the EDC's for $h\nu > 20$ eV was to obtain information on possible contributions from core d levels (the $4d$ level of Sb). Our results show no core d bands in the 7–30-eV region, which indicates that the optical properties of Sb_2Se_3 in Ref. 4 are due to the s and p valence electrons only.

Since there is present a large amount of structure in our data as a result of strong polarization dependence, a large span of photon energy, and a complex band structure, it is advantageous to identify briefly the most prominent structures in Figs. 1–6. Analysis of the EDC's shows that most of the structure can be related to the constant energy of either initial or final states. Therefore, two sets of EDC's are presented: one with EDC's arranged with respect to the initial energy, suitable for determining the valence-band structure, and the other set arranged with respect to the final-state energy, suitable for determining the conduction-band structure.

The structure of constant initial-state energy

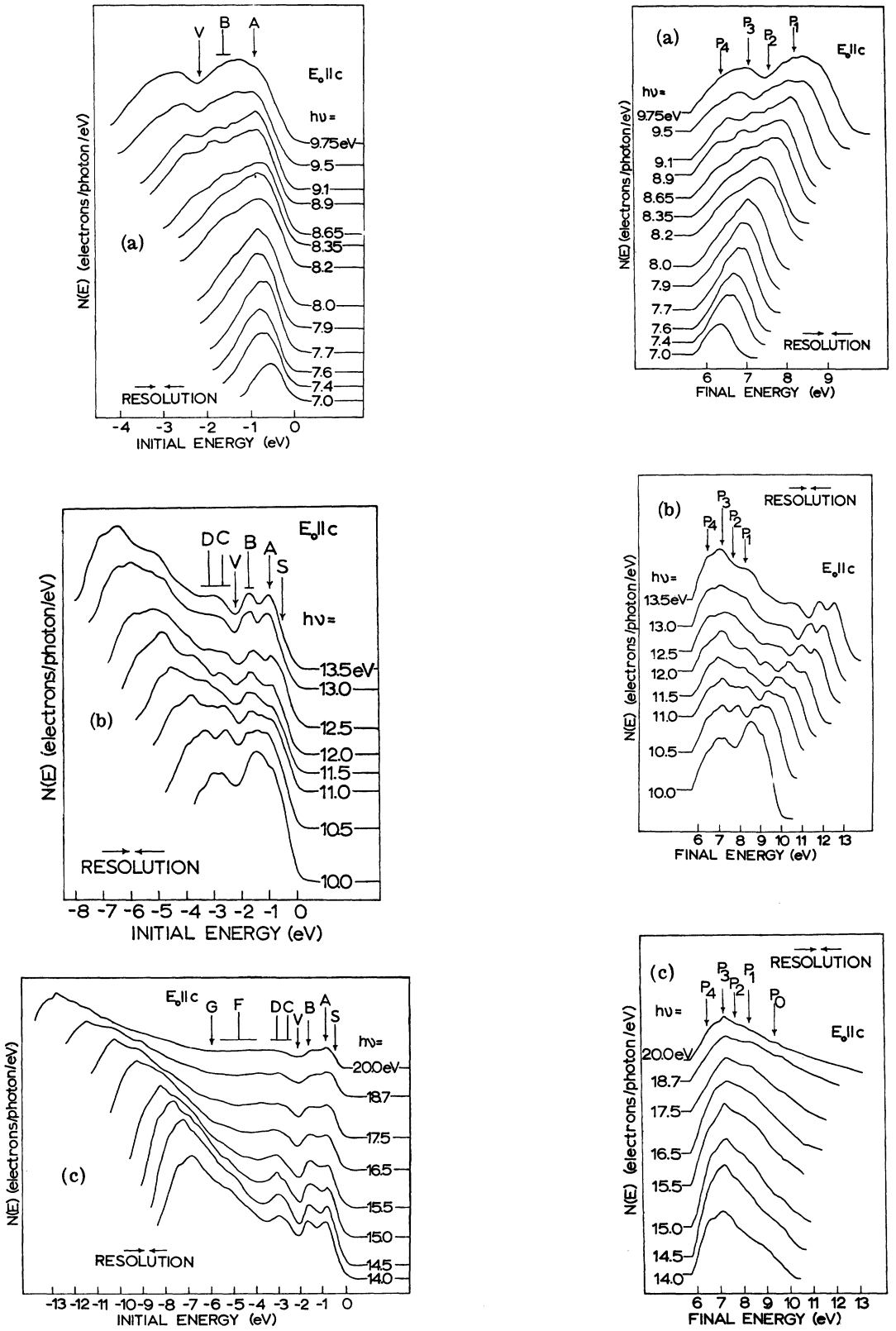

FIG. 1. Energy-distribution curves (EDC's) for $\vec{E}_0 \parallel \hat{c}$, with respect to the initial states.

FIG. 2. EDC's for $\vec{E}_0 \parallel \hat{c}$, with respect to the final states.

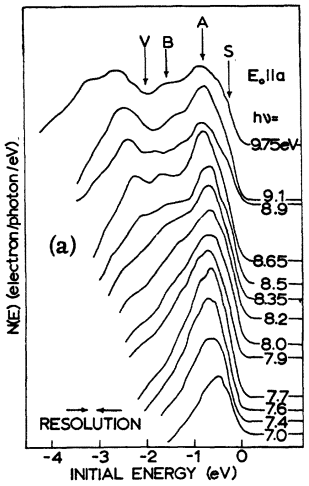

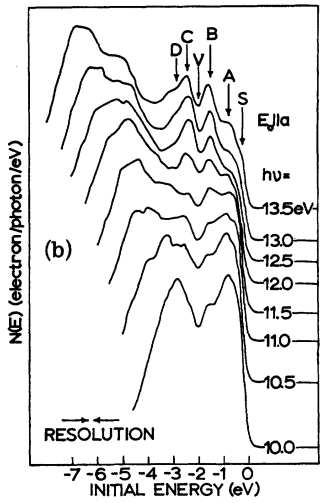

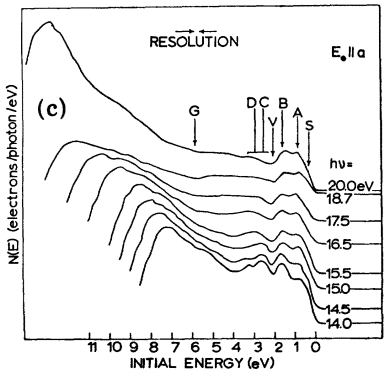

FIG. 3. EDC's for $\vec{E}_0 \parallel \hat{a}$, with respect to the initial states.

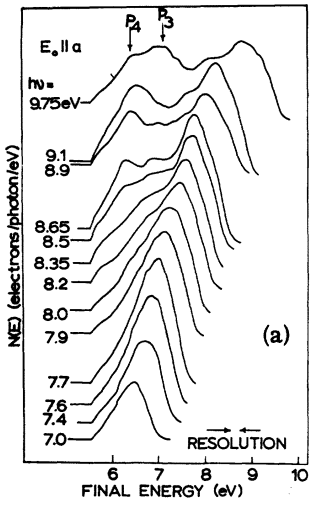

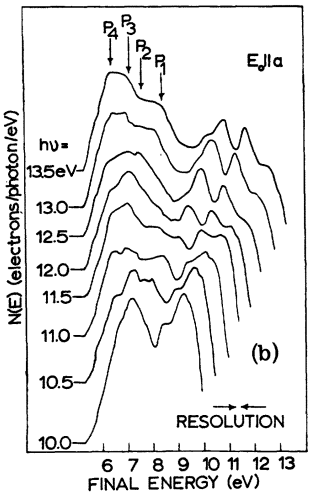

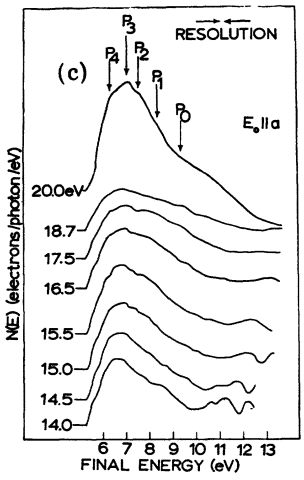

FIG. 4. EDC's for $\vec{E}_0 \parallel \hat{a}$, with respect to the final states.

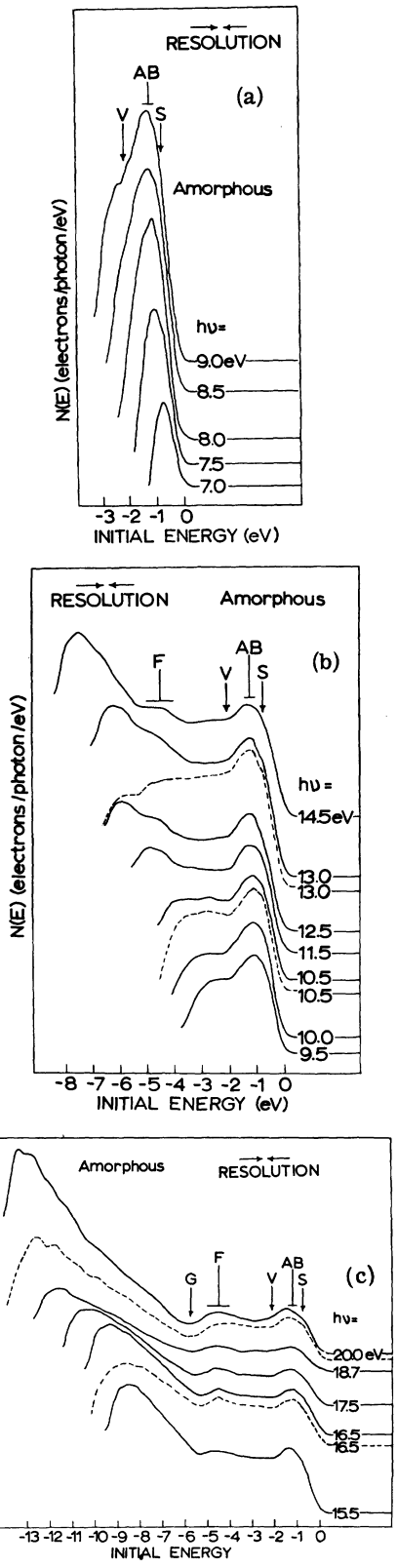

FIG. 5. EDC's for amorphous Sb_2Se_3, with respect to the initial states.

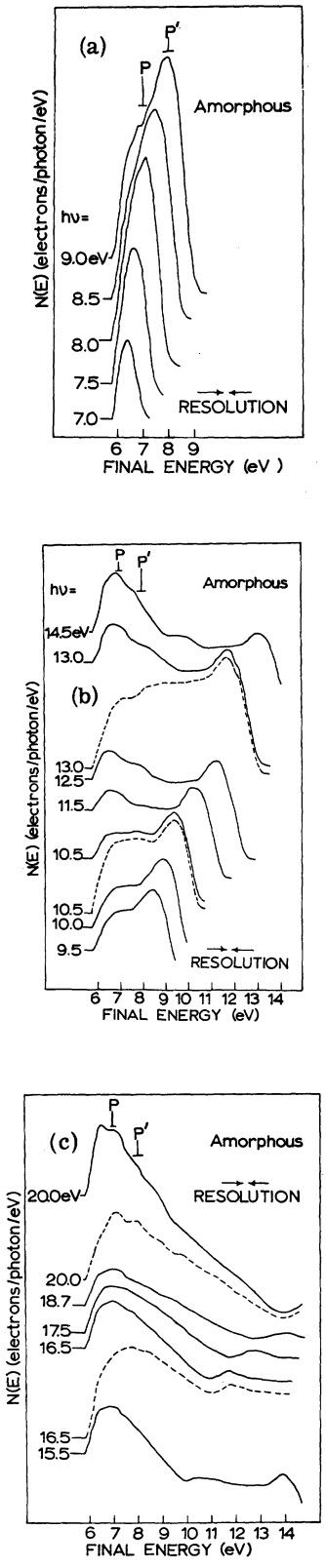

FIG. 6. EDC's for amorphous Sb_2Se_3, with respect to the final states.

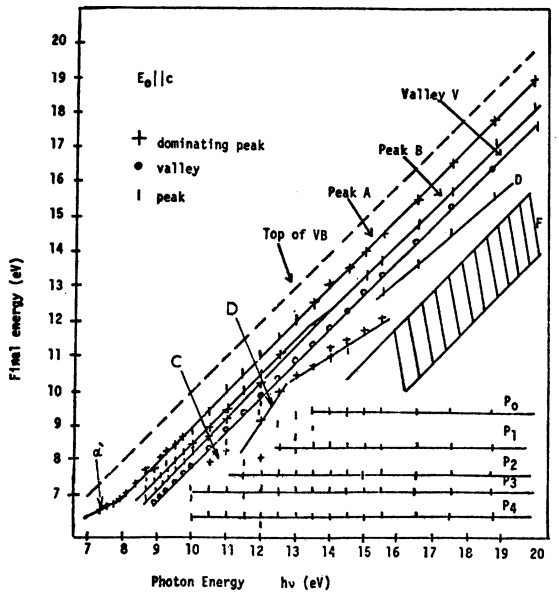

FIG. 7. Structure plot for $\vec{E}_0 \| \hat{c}$.

(Figs. 1, 3, and 5) includes a weak shoulder S on the sharp leading edge, and two sharp peaks A and B in crystalline Sb_2Se_3 (or one broad peak AB in amorphous Sb_2Se_3) at the high-energy end of EDC's for $h\nu$ in the 8–20-eV range; these structures are separated from the rest of the EDC's by a valley V located 2 eV below the high-energy end of the EDC's. Additional peaks C and D are located at ~0.6 and 1.3 eV below the valley V for crystalline Sb_2Se_3. The structure with the constant final-state energy (Figs. 2, 4, and 6) is observable at the low-energy end of the EDC's. It includes five shoulders and peaks P_0 to P_4 in crystalline Sb_2Se_3, and two structures P and P^1 in amorphous Sb_2Se_3. For further presentation and analysis of the EDC's we have used the standard method of structure plots where the final energy E of each element of the structure is plotted vs the photon energy $h\nu$ (Figs. 7–9), with the energies referred to the valence-band maximum (VBM). The high (and energy-independent) resolution of the analyzer used provides rather sharp leading edges of the EDC's which can be easily extrapolated to zero emission intensity to define the top of the valence band. The very weak tail at the high-energy end of the EDC's is due to both intrinsic broadening (as a result of the electric field penetration) as well as to the instrumental broadening (nonuniform work function of the analyzer, finite bandwidth of the exciting radiation, finite resolution of the analyzer).

V. CRYSTALLINE Sb_2Se_3

A. $\vec{E}_0 \| \hat{c}$

In the region between the threshold energy and $h\nu = 8$ eV, a peak in the EDC's occurs close to the top of the valence band (Fig. 1, also line α' in Fig. 7). This structure is attributed to direct transitions since it does not correspond to the slope of the $E = h\nu$ line in the structure plot (Fig. 7) and ends at $h\nu = 8$ eV. At $h\nu = 8$ eV a sharp peak A occurs in the EDC. Figs. 1 and 7 show that this peak keeps a constant energy of initial states in the entire photon-energy range up to 20 eV, but the intensity of this peak is strongly varying with $h\nu$; in the 9.5–11.5-eV range this peak almost disappears. Another structure of constant energy of the initial states is peak B, starting at $h\nu \sim 8.6$ eV as a weak shoulder. The intensity of this peak is again strongly varying with photon energy. The high resolution of this experiment shows this peak,

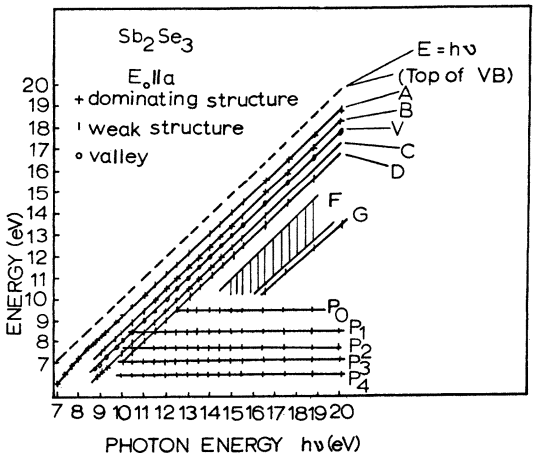

FIG. 8. Structure plot for $\vec{E}_0 \| \hat{a}$.

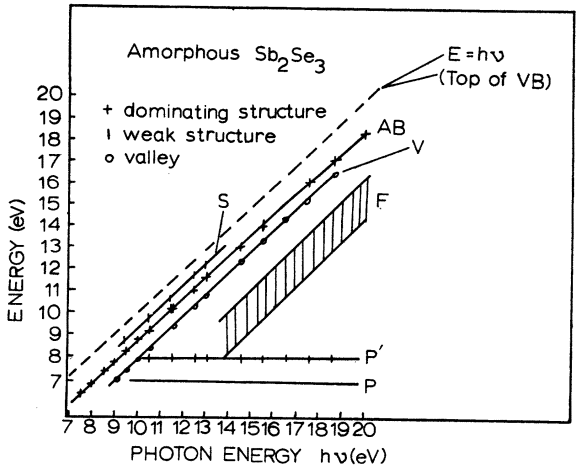

FIG. 9. Structure plot for amorphous Sb_2Se_3.

B, as a doublet ~0.3 eV wide in the $h\nu \sim 9$–13-eV region. A weak shoulder S on the leading edge of most of the EDC's can also be observed. Peaks A and B are separated from the remaining part of the EDC's by a valley V at 2 eV below VBM. This valley V is one of the most prominent features of EDC's for crystalline Sb_2Se_3. Since the two peaks A and B occur in an extremely large photon energy range (~20 eV) with constant and well-defined initial energy, we conclude that they correspond to high-density-of-states regions in the valence band arising from flat E-vs-k parts of the band. In the $h\nu = 8$–15-eV region the intensity of these two peaks is strongly varying with $h\nu$ owing to the effect of matrix elements. In the case of optically isotropic materials, this feature would be a clear indication of direct, i.e., $\vec{k}$-conserving, optical transitions. In the case of such a strongly anisotropic material as Sb_2Se_3 it is possible, however, that this matrix-element modulation could be due to the $\vec{E}_0$ rather than the $\vec{k}$ dependence of matrix elements. Therefore the only definite indication that the transitions are direct is that the slope differs from 45° in the structure plot for peak A in the small photon-energy range between the threshold and 8 eV.

Starting at $h\nu \sim 10$ eV, Fig. 1 shows two other peaks, C and D, of strongly varying intensity in the region 0.4–1.3 eV below the valley V. A slope differing from the $E = h\nu$ slope in the corresponding structure plot (Fig. 7) indicates that these peaks are associated with direct optical transitions. There is a suggestion of another deeper-lying structure in the valence band (labeled F), obscured by the background of inelastically scattered electrons and by the overlapping conduction-band structure. This background is also partially obscuring an onset of another region of high density of states starting at about 6 eV below VBM (point G in Fig. 1) for EDC's at $h\nu > 15.5$ eV. We suggest that the sharp change of the slope at point G corresponds to an increase of the valence-band densities of states, yet superimposed on a background of conduction-band structure and scattered electrons since (i) point G corresponds to a constant energy of initial states and is therefore a property of the valence band, and (ii) the inelastically scattered electrons would form a smooth background dependent on the final rather than on initial energies. In amorphous Sb_2Se_3 (Fig. 5) this deeper new band is much better resolved in the EDC's owing to much weaker conduction-band structure (Fig. 5). This assignment of point G to the onset of a deeper valence band is further confirmed by the x-ray photoemission spectra,[6] which portrays the structure of the occupied states.

The conduction-band structure can be conveniently determined from the EDC's arranged with respect to the final energies of photoelectrons (Fig. 2). Five regions of higher density of states (labeled P_0 to P_4) superimposed on a background of inelastically scattered electrons can be determined from Fig. 2 between 6 and 10 eV above the VBM. In general, such conduction-band density-of-state maxima can be filled either directly by optical excitation, or by photoexcited electrons which are inelastically scattered down from higher energies.[19] Since the intensity and shape of these five peaks or shoulders is strongly dependent on the photon energy, these structures in the EDC's obviously correspond to the optically excited electrons rather than to the filling of these states by scattered electrons. This is best shown by observing the crossings of the lines representing the peaks A, B, C, and D with lines representing P_0 to P_4 in the structure plot (Fig. 7). At several photon energies, corresponding to these crossings, strong interband optical transitions, enhanced by high densities of states in both bands, occur and show up in the EDC's as strong peaks, modulated further by the matrix elements $M(h\nu, \vec{k}, \vec{E}_0)$. For $\vec{E}_0 \| \hat{c}$, such strong peaks in the EDC's occur for example at $h\nu = 8$ eV (transition from A to P_3) and $h\nu = 10$ eV (from B to P_1). A complete list of such transitions is given in Table I.

The lower part of the conduction band is not accessible owing to the photoelectric threshold of ~5.9 eV, as determined from the spectral distribution of the yield Y using a linear $(Y\ h\nu)^{3/2}$-vs-$h\nu$ extrapolation.[20]

B. $\vec{E}_0 \| \hat{a}$

The EDC's for $\vec{E}_0 \| \hat{a}$ (Figs. 3 and 4) bear resemblance to EDC's for $\vec{E}_0 \| \hat{c}$. The high-energy side of the EDC's shows four peaks, A, B, C, and D, of constant and rather well-defined initial-state energy (Figs. 3 and 8). A shoulder S can be observed on the leading edge of EDC's. These four peaks are attributed again to the valence-band density-of-states maxima originating from flat E-vs-k portions of the band. In the EDC's these maxima are then strongly modulated by the matrix elements $M(h\nu, \vec{k}, \vec{E}_0)$. For example, the very sharp peak A at 10 eV is changing into a very weak shoulder in the 11.5–15-eV region.[21] Peaks A and B are again clearly separated from the rest of the EDC's by the valley V located 2 eV below VBM, which is also one of the most prominent features of the EDC's for $\vec{E}_0 \| \hat{a}$. A weak structure F and an onset of a deeper valence band at G are also observed in Fig. 3. Contrary to the $\vec{E}_0 \| \hat{c}$ polarization, peaks C and D keep a constant initial-state energy in this polarization for the entire photon-energy range where they are present (see also Fig. 8). Five regions P_0 to P_4 of high density of states in the conduction band are observed in the low-energy side of the EDC's (Fig. 4) superim-

TABLE I. Position of the density-of-states maxima in (eV) with respect to the VBM.

Crystalline Sb_2Se_3	Amorphous Sb_2Se_3
$A \sim 0.8$	$AB \sim 1.2$
$B \sim 1.6$	
$C \sim 2.6$	
$C \sim 3.3$	
$P_4 \sim 6.4$	
$P_3 \sim 7.2$	$P \sim 7$
$P_2 \sim 7.8$	
$P_1 \sim 8.5$	$P' \sim 8$
$P_0 \sim 9.3$	

posed on a smooth background of scattered electrons. These conduction-band densities are again coupled in optical transitions from the states in the upper valence band (Table II).

Comparing the EDC's for $\vec{E}_0 \| \hat{a}$ with $\vec{E}_0 \| \hat{c}$ shows the dependence of the relative intensity of these peaks on the orientation of $\vec{E}_0$ (see Fig. 10). This indicates that the matrix elements include dependence on both $\vec{k}$ and $\vec{E}_0$, the latter dependence arising as a result of the crystal-field effect. Owing to the differential character of the photoemission method, this $\vec{E}_0$ dependence is much more pronounced in the EDC's than in the reflectance data (Fig. 11). The EDC's are strongly polarization dependent in the photon energy range from 8 to ~15 eV, where the reflectance shows very little polarization dependence. While, for example, the reflectivity and the optical transition strength $\omega^2\epsilon_2$ (i.e., JDOS) exhibit the same two peaks at ~10 and 12.5 eV for both polarizations (Fig. 11) the EDJDOS (the energy distribution of JDOS) is quite different for these two polarizations (Fig. 10). The reflectivity peak at ~10 eV has a strong contribution from peak A in EDC's for $\vec{E}_0 \| \hat{a}$ and from peak B for $\vec{E}_0 \| \hat{c}$. The reflectivity peak at ~12.5 eV has a large contribution from peaks B and C in EDC's for $\vec{E}_0 \| \hat{a}$, and approximately equal contributions from A and B for $\vec{E}_0 \| \hat{c}$. It is primarily the upper 3 eV of the valence band which produces a strong polarization and photon energy dependence of the EDJDOS which is not detectable in the reflectance data.

TABLE II. Polarization dependence of the transition between the valence-and conduction-band DOS maxima in crystalline Sb_2Se_3.

$h\nu$ (eV)	Transition	$\vec{E}_0 \| \hat{a}$	$\vec{E}_0 \| \hat{c}$
8.0	$A \rightarrow P_3$	Weak	Strong
10.1	$B \rightarrow P_1$	Weak	Strong
10.1	$D \rightarrow P_3$	Strong	Weak
10.6	$D \rightarrow P_1$	Weak	Strong
12.0	$C \rightarrow P_0$	Strong	Not observed

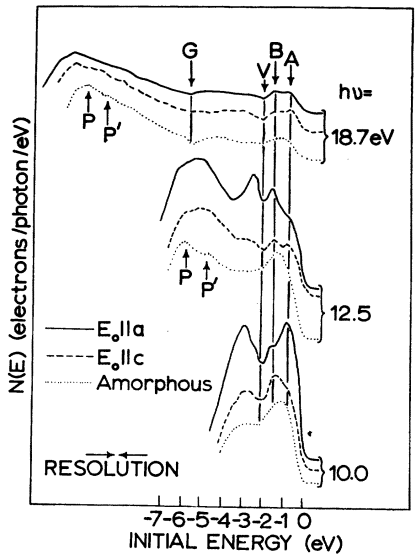

FIG. 10. Polarization dependence of the EDC's.

VI. AMORPHOUS Sb_2Se_3

The total photoemission yield of amorphous Sb_2Se_3 films was lower than that of crystalline Sb_2Se_3, and the low-energy part of the EDC's was partially obscured by the background of photoelectrons emitted from the analyzer.[22] A correction for this effect at several photon energies is shown in Figs. 5 and 6 (dashed lines). These corrected EDC's still include, however, the secondary (scattered) electrons originating in the conduction band of Sb_2Se_3 films.

The structure of the EDC's for amorphous Sb_2Se_3 is much less complicated than for the crystalline form, yet the main features are similar. There is again a shoulder S and a peak AB at the high-

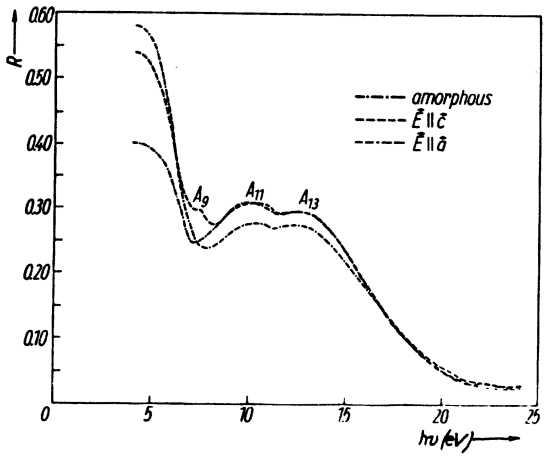

FIG. 11. Reflectance spectrum of Sb_2Se_3 (after Ref. 4).

energy end separated from the rest of the EDC's by the valley V. However, the two very sharp peaks A and B in crystalline Sb_2Se_3 are now replaced by the broad peak AB, and the peaks C and D at the low-energy side of V are completely missing. Both peak AB and valley V indicate again a constant initial-state energy which is primarily attributable to the valence-band structure. Of particular interest are the changes of the shape of the EDC's at $h\nu = 8$ and 9 eV, where some sharpening of the peak AB occurs. The occurrence of such sharp peaks is rather unusual for an amorphous material, and in this case it is plausible to explain such peaks in the EDC's by a high density of states in the conduction band. Figures 6 and 9 indeed show two weak regions of high densities of states, P and P', in the conduction band at ~7 and 8 eV above the top of the valence band. Their energy position corresponds to regions P_2 and P_3 of high densities of states in crystalline Sb_2Se_3, but their intensity is much weaker. The weakness of the conduction-band structure in amorphous Sb_2Se_3 is a property of the amorphous films, rather than an instrumental resolution effect, since the lower part of the valence band (point G) is resolved more sharply in amorphous than crystalline Sb_2Se_3 despite the lower yield of films. Similar smoothing of the high density of the conduction-band states in the amorphous phase of Se and Te have been reported by Laude and Fitton.[23] Results[18] indicate that the difference between EDC's for crystalline and amorphous Sb_2Se_3 is *not* due to collecting electrons under a specific solid angle, which would average out the structure in amorphous Sb_2Se_3.

Since the only two appreciable changes of the shape of the peak AB in the EDC's at $h\nu \sim 8$ and 9 eV can be explained by the higher conduction-band density of states, the otherwise constant shape and relative intensity of the peak AB suggest that it is due to nondirect transitions. It is interesting to note that within the resolution (0.2 eV) of the experiment, both crystalline and amorphous Sb_2Se_3 exhibit very sharp high-energy ends of the EDC's; in particular, there is no direct evidence of the density of states tailing in amorphous stoichiometric Sb_2Se_3, in agreement with previous findings from the optical and photoconductivity data.[24]

VII. DISCUSSION

One important feature of the EDC's is the strong structure in their upper 2-eV region. In the case of crystalline Sb_2Se_3, this region is strongly polarization dependent and split into peaks A and B, and is clearly separated from the rest of the EDC's by the valley V. The peaks A and B are rather narrow, their full width at half-maximum above the valley V being ~0.4 eV. Such narrow bands would be consistent with rather low hole mobility, ~40 cm^2/V sec,[25] in crystalline Sb_2Se_3. We associate these two peaks A and B with two regions of valence-band density-of-states maxima arising from flat E-vs-k bands. In agreement with this interpretation, the energy position of these two peaks from the VBM is the same for both polarizations. In the EDC's these valence-band density-of-states maxima are modulated by the matrix elements $M(h\nu, \vec{k}, \vec{E}_0)$, and to some extent by the escape function S and also by the conduction-band density of states for $8 < h\nu < 15$ eV. In view of the atomic-states configuration of Sb and Se, these flat bands are attributed primarily to p electrons, which would be rather localized at atoms, peaks A and B in the EDC's of crystalline Sb_2Se_3 merge into one broad peak AB in amorphous Sb_2Se_3. This peak AB does not allow for a very flat E-vs-k band, and its behavior suggests that it is due to nondirect transitions with constant matrix elements, modulated by the conduction-band density of states at $h\nu \sim 8$ and 9 eV.

The other portion of the valence band being strongly affected by the phase transition is located between 2.0 and 3.3 eV below the VBM in crystalline Sb_2Se_3 (peaks C and D in the EDC's). Optical transitions from these states are again strongly dependent on the orientation of $\vec{E}_0$. Behavior of these peaks in the structure plot (Fig. 7) for $\vec{E}_0 \| \hat{c}$ again indicates that the corresponding optical transitions are direct in crystalline Sb_2Se_3. In the EDC's for amorphous Sb_2Se_3 these two peaks C and D are completely missing.

Even though the effect of polarized light on the EDC's in the case of optically anisotropic materials has been reported earlier,[13,16,26] the effects observed here are far stronger. It is also interesting to note that the polarization dependence is strongest for electrons excited from flat bands at the upper ~3-eV part of the valence band. In view of the discussion in the theoretical section, it is believed that this strong polarization dependence of the EDC's is due primarily to the M_{if} term, with the S term giving possibly a weak background dependence such as observed in the EDC's at $h\nu > 16$ eV. Even though a rigorous proof of this statement requires a detailed knowledge of the band structure, there are some experimental facts in its support: (i) The reflectance spectra in the visible range shows clearly strong $M_{if}(\vec{E}_0)$ dependence for states within the upper ~3 to 4 eV of the valence band, and (ii) the main features of the EDC's are independent of the type of analyzer used.[18] This observed $\vec{E}_0$ dependence of M_{if} shows the effect of crystal field and symmetry. The strong polarization dependence of EDC's makes it difficult to determine whether the transitions are direct, since the strong $\vec{E}_0$ dependence of M_{if} obscures any possible $\vec{k}$ dependence. There are in-

dications of direct transitions, such as the slope in the structure plots, but only in a limited range of $h\nu$ (e.g., peaks C and D for $\vec{E}_0 \| \hat{c}$ in Fig. 7). The question of direct transitions is further complicated by the flatness of the bands corresponding to the initial states.

An additional increase of the density of states for both crystalline and amorphous Sb_2Se_3 starts ~6 eV deep in the valence band (point G), which is seen as a sharp change of the slope of the EDC's in Figs. 1, 3, and 5 at $h\nu > 17.5$ eV. It is reasonable to assume that this lower portion of the valence band contributes significantly to the reflectivity rise at $h\nu \sim 7$ eV even though the onset of these transitions cannot be seen in the EDC's due to the work-function limitation.

The conduction band shows five closely spaced regions of higher densities of states between 6.5 and 9.5 eV above VBM (P_0 to P_4) for both polarizations in crystalline Sb_2Se_3, and two weak structures, P and P', at about 7 and 8 eV for amorphous Sb_2Se_3. The energy position of these conduction-band densities of states and their coupling in optical transitions to various regions of the valence band are presented in Table II. The existence of these conduction-band densities of states in Sb_2Se_3 has further been confirmed by comparing the optical transition strength $\omega^2\epsilon_2$ with the x-ray photoemission spectroscopy (XPS).[6] One interesting feature of the conduction-band structure is that it shows up much weaker for amorphous than for crystalline Sb_2Se_3. This can be explained by the lack of matrix-element enhancement, or by a strong effect of the long-range disorder on the higher conduction band. In particular, the effect of the long-range disorder on the smoothing of the conduction-band structure is much stronger than on the sharpness of the valence-band edge.

At higher photon energies ($h\nu > 16$ eV), the high-energy end of the EDC's changes very little with $h\nu$, and similar to other works,[27,28] portrays the basic feature of the valence-band density of states (DOS). The derived model DOS's for crystalline and amorphous Sb_2Se_3 are presented in Fig. 12. The relative intensity of the individual peaks in this model cannot be determined accurately owing to several unknown factors, like M_{if} and S. Since the scattering length necessary to subtract the low-energy peak due to inelastically scattered electrons is not available, the model densities in Fig. 12 are "normalized" with respect to the optical sum rules from Ref. 4; also some cross features of the XPS spectra[6] are used in this model. It is interesting to note that owing to improved resolution, the EDC's reveal more detailed structure (e.g., the valley V) in the densities of states for crystalline and amorphous Sb_2Se_3 than the XPS data.[6]

Since the valley V, separating the upper 2 eV of the valence band, is one of the most prominent features of EDC's for both polarizations, some physical interpretation of this structure is appropriate. This can be done by application of the optical sum rules, which determines that there are six electrons per molecule located between the VBM and the valley V participating in the optical transitions from $h\nu = 1.2$ eV (the bandgap of Sb_2Se_3) to $h\nu = 3.2$ eV. Certain caution has to be exercised when using the optical sum rules, since it provides the "effective number" as determined from the total oscillator strength. This effective number can differ from the true number of valence electrons, particularly when the upper limit $h\nu$ lies within the region of optical transitions. This has been observed in the case of Ge and III-V compounds due to the core d-level contribution to the total oscillator strength.[29] In Sb_2Se_3, however, the highest occupied levels are the Sb $4d$ states ~33 eV below the VBM,[6] and the optical sum rules up to $h\nu = 25$ eV do not exhibit any contribution due to these d-bands.[4] Therefore, within the numerical accuracy of the optical sum rules,[30] we consider n_{eff} as a reasonable and useful first-order approximation.

Since no band-structure calculations have been done for Sb_2Se_3 or similar orthorhombic V-VI compounds (primarily owing to its very complicated primitive cell containing 112 valence electrons), the only theoretical model for the electronic structure of Sb_2Se_3 at present is the conjecture resulting from the molecular-orbital approach.[5,31] Our results can then be interpreted in the following way: The upper part (first 6 eV) of the valence band is attributed to weakly bonding states which

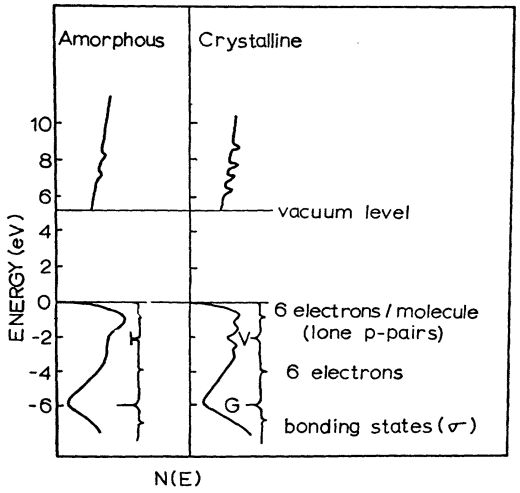

FIG. 12. Model density of states for Sb_2Se_3.

have strong p-like character as evidenced by several flat bands. According to the sum-rule calculation[4] it includes a total of 12 electrons per Sb_2Se_3 molecule with six electrons per molecule being located within the upper 2-eV region between the VBM and the valley V. These six electrons per molecule can be attributed primarily to the three lone (unshared) p pairs of selenium electrons[32] whose existence in this class of compounds has been suggested by Kastner.[5] At this point it should be mentioned that such separation of the group of ~6 electrons per molecule by the valley V in the EDC's-derived DOS was found also for other V-VI crystals, Bi_2Te_3 and Sb_2Te_3, of rhombohedral $D3m$ structures,[33] and seems to be a general feature of the V-VI compounds, indicating the presence of the lone p pairs. Also we would like to note the striking similarity of the DOS model of Sb_2Se_3 to those of Shevchick *et al.* for Se,[28] particularly the separation of the lone-pair band. This suggests the important role of the lone pairs of chalcogen atoms in forming the weakly bonding band of VB_2VIB_3 compounds. The lone-p-pair band in orthorhombic Sb_2Se_3 is further split by the crystal field (peaks A and B) resulting from the low symmetry; this splitting is not observed in trigonal Se. Whereas the entire nonbonding band of VB_2VIB_3 compounds has been previously referred to as the "lone-pair band,"[5] the combination of the photoemission and XPS data, together with the sum rules, shows that, in addition to the three lone pairs, this nonbonding band contains approximately another six electrons per molecule, clearly separated from the lone pair by the valley V. Similarly to the lone p pairs those deeper states have again a strong contribution from the flat E-vs-k band (peaks C and D), indicating strong p character with a large contribution probably from the Sb $5p$ states.

The lower part of the valence band (bonding) starting at about 6 eV below VBM arises from the bonding states and corresponds to the σ orbitals of the molecular states. According to the sum rule[4] this band, including 16 electrons per molecule, can extend up to 25 eV below the VBM. This band should include the remaining p states of Se and Sb, $5s$ states of Sb, and possibly the deep $4s$ states of Se. Owing primarily to the difference in the strength of the conduction-band structure, the onset of this bonding band is resolved better in the EDC's for amorphous than for crystalline Sb_2Se_3. In the x-ray-photoemission spectrum, which is sensitive primarily to the valence-band structure, the onset of this band is resolved equally well for both amorphous and crystalline Sb_2Se_3.[6] The $4d$ states of Sb, according to present results as well as to Refs. 4 and 6, do not contribute to this band.

The lowest part of the conduction band would correspond to σ^* antibonding molecular states. The EDC's show several additional regions of well-localized higher densities of states in the conduction band in the region 6–10 eV above the VBM superimposed on a more or less smooth conduction band. The small width of these states and their strong optical coupling to the p-type states at the upper (weakly bonding) valence band suggests d-like character of these higher conduction states, P_0 to P_4. The intensity and sharpness of these states is much lower in the amorphous phase.

It would be very interesting to correlate the electronic states to the different types of bonds, particularly in regard to different bond strengths in the case of this pseudo-two-dimensional crystal consisting of Sb_4Se_6 units.[34] The x-ray-diffraction data of Tideswell *et al.*[34] show that the bond character is very complex since the bond distances occur anywhere between the sum of covalent radii ~2.6 Å and ~3.8 Å (the sum of the van der Waals radii for Sb and Se is 4.20 Å). The six electrons in the upper 2 eV (primarily lone pairs) of the weakly bonding band can be considered to play some role in forming the six weakest bonds per molecule (bond distances 3.74 and 3.46 Å) holding the crystal layers together and only a small amount of the electronic charge participates in forming the bonds, as the bond number is ~0.01. The crystal field and symmetry determine the direction of these bonds and their energy levels (rather flat E-vs-k bands giving rise to peaks A and B) so that the total crystal energy is minimized. Another six weak bonds per Sb_2Se_3 molecule (bond distances 3.26 and 3.27 Å, bond number ~0.1) responsible for bonding infinitely long Sb-Se chains into crystal layers can be associated, at least in part, with another six weakly bonding electrons located between the valley V and the point G. The direction of these bonds and corresponding electronic energy levels are again determined by the crystal field, which shows up in the EDC's via the strong $\vec{E}_0$ dependence of matrix elements. The σ (bonding) states are involved in forming the strong Sb-Se bonds of distance 2.57–2.98 Å (bond number ~1.0) within infinitely long chains, parallel with the c axis.[34]

In amorphous Sb_2Se_3 these weakly bonding states are determined by the local potential instead of the crystal field. The weak bonds, responsible formerly for holding together or forming the crystal layers, are now randomly oriented in space, and their energy levels, determined locally, lose their resonant character and the bands consequently become wider. This is clearly reflected in the EDC's for amorphous Sb_2Se_3, where the sharp peaks A and B are replaced by one broad peak AB, and peaks C and D are completely missing. The

separation of the lone pairs by the valley V from the rest of the weakly bonding band is also very weak in amorphous Sb_2Se_3.

The effect of the crystal field and the similarity between the major features of the DOS of crystalline and amorphous Sb_2Se_3 are consistent with the model of both phases displaying properties characteristic of molecular solids, the crystal containing Sb_4Se_6 units bonded rather weakly to one another[34] and amorphous films being a random aggregate of Sb_4Se_6 molecules.[35]

VIII. CONCLUSION

The EDC's present a considerable extension of the DOS model derived from the general molecular-orbital approach. It is shown that the upper ~3-eV region of the weakly bonding band has a strong p-type character with flat bands, whose states are strongly affected by the crystal field as evidenced by a strong polarization dependence of matrix elements. This region of the valence band is also very strongly affected by the transition to the amorphous phase, where the local potential results in smearing of the fine details of the valence-band DOS. The similarity between the lone-pair bands in the DOS of Sb_2Se_3 and Se[28] suggests the role of the chalcogen lone p-pairs in forming the weakly bonding band of Sb_2Se_3 and other VB_2VIB_3 compounds.

---

*Work supported by the Advanced Research Projects Agency of the Department of Defense and was monitored by the Army Research Office, Durham, under Contract No. DA-ARO-D-31-124-71-G132. We wish, also, to acknowledge the support of the Synchrotron Radiation Laboratory, University of Wisconsin, under Air Force Contract No. F44620-70-C-0029.

†Supported by Air Force Office of Scientific Research, Office of Aerospace Research, USAF, under Grant No. AFOSR-71-2061.

[1]K. Murase, J. W. Osmun, J. Freeouf, M. Kastner, and C. Wood, Bull. Am. Phys. Soc. 17, (No. 3) 345 (1972).

[2]S. D. Shutov, V. V. Sobolov, Y. V. Popov, and S. N. Shestatskii, Phys. Status Solidi 31, K 23 (1969).

[3]R. Zallen, R. E. Drews, R. L. Emerald, and M. L. Slade, Phys. Rev. Lett. 26, 1564 (1971).

[4]J. C. Shaffer, B. Van Pelt, C. Wood, J. Freeouf, K. Murase, and J. W. Osmun, Phys. Status Solidi B 54, 511 (1972).

[5]M. Kastner, Phys. Rev. Lett. 28, 6 (1972); 28, 355 (1972).

[6]C. Wood, J. C. Shaffer and W. G. Proctor, Phys. Rev. Lett. 29, 485 (1972).

[7]G. J. Lapeyre, A. D. Baer, P. L. Gobby, and C. F. Badgley (unpublished).

[8]C. Wood, B. Van Pelt, and E. Hyland, Rev. Sci. Instrum. 43, 1374 (1972).

[9]R. Mueller and C. Wood, J. Noncryst. Solids 7, 301 (1972).

[10]W. F. Krolikowski and W. E. Spicer, Phys. Rev. 185, 882 (1969).

[11]J. F. Janak, O. E. Eastman, and A. R. Williams, Solid State Commun. 8, 271 (1970).

[12]N. V. Smith, Phys. Rev. B 5, 4 (1972); 5, 1192 (1972).

[13]G. F. Derbenwick, Ph. D. thesis (Stanford University, 1970) (unpublished).

[14]U. Gerhardt and E. Dietz, Phys. Rev. Lett. 26, 1477 (1971).

[15]T. Gustafssons, P. O. Nilsson, and L. Wallden, Phys. Lett. A 37, 121 (1971).

[16]R. Y. Koyama and L. R. Hughey, Phys. Rev. Lett. 29, 1518 (1972).

[17]G. D. Mahan, Phys. Rev. B 2, 4334 (1970).

[18]EDC's of Sb_2Se_3 taken with the retarding-field analyzer and the electrostatic double-pass cylindrical-mirror analyzer support this criterion. There is some difference in the relative intensity of the peaks taken with the two different analyzers, but this difference varies rather smoothly with photon energy. Z. Hurych, D. Davis and T. Knecht (unpublished).

[19]R. A. Powell, W. E. Spicer, and J. C. McMenamin, Phys. Rev. B 6, 3050 (1972).

[20]J. M. Ballantyne, Phys. Rev. B 6, 1436 (1972).

[21]It is possible that this weak shoulder is due to the nonpolarized component (approx. 20%) of the radiation and that it would disappear if 100% polarized radiation were used. [B. Van Pelt (private communication).]

[22]Even though the analyzer used detects only the electrons originating at its focal point, it is not able to discriminate against electrons emitted from other parts of space yet having a virtual origin at its focal point. Most of the background electrons come from the two illuminated concentric screens used to define the field-free region and the region of acceleration or deceleration.

[23]L. D. Laude and B. Fitton, J. Noncryst. Solids 8–10, 971 (1972).

[24]Z. Hurych, C. Wang, R. Mueller and C. Wood, J. Noncryst. Solids 11, 153 (1972).

[25]J. Black, E. M. Conwell, L. Seigle, and C. W. Spencer, J. Phys. Chem. Solids 2, 240 (1957).

[26]G. J. Lapeyre, T. Huen, and F. Wooten, Solid State Commun. 8, 1233 (1970).

[27]W. D. Grobman and D. E. Eastman, Phys. Rev. Lett. 29, 1508 (1972).

[28]N. J. Schevchnik, J. Tejeda, M. Cordona, and D. W. Langer, Solid State Commun. 12, 1285 (1973).

[29]H. R. Phillip and H. Ehrenreich, Phys. Rev. 129, 1550 (1963).

[30]5 to 10% [J. C. Shaffer (private communication)].

[31]E. Mooser and W. B. Pearson, J. Phys. Chem. Solids 7, 65 (1958).

[32]Z. Hurych, D. Buczek, C. Wood, G. J. Lapeyre, and A. D. Baer, Solid State Commun. 13, 823 (1973).

[33]Z. Hurych, D. Davis, and T. Knecht, Bull. Am. Phys. Soc. 19, 78 (1974).

[34]N. W. Tideswell, F. H. Kruse, and J. C. McCullough, Acta Cryst. 10, 99 (1957).

[35]Z. Hurych, J. C. Shaffer, C. Wood, J. G. Lapeyre, and A. D. Baer, Proceedings of the Fifth International Conference on Amorphous and Liquid Semiconductors September, 1973 (unpublished).